CONICAL NEAR-FIELD ANTENNA MEASUREMENTS

Stuart F. Gregson, Greg E. Hindman
Nearfield Systems Inc.
19730 Magellan Drive,
Torrance, CA 90502-1104

ABSTRACT

A near-field measurement technique for the prediction of asymptotic far-field antenna patterns from data obtained from a modified cylindrical, or plane-polar, near-field measurement system is presented. This technique utilises a simple change in facility alignment to enable near-field data to be taken over the surface of a conceptual right cone [1, 2], or right conic frustum [3, 4] thereby allowing existing facilities to characterise wide-angle antenna performance in situations where hitherto they would perhaps have been limited by truncation.

This paper aims to introduce the measurement technique, describe the novel probe-corrected near-field to far-field transform algorithm which is based upon a cylindrical mode expansion of the measured fields before presenting preliminary results of both computational electromagnetic simulations and actual range measurements. As this paper recounts the progress of ongoing research, it concludes with a discussion of the remaining outstanding issues and presents an overview of the planned future work.

Keywords: Near-Field, Antenna Measurements, Conic Frustum, Cylindrical.

1. Introduction

It is well known that far-field antenna parameters such as pattern, gain, directivity, beamwidth, *etc.*, can be derived from near-field measurements. For such parameters, which are not obtained directly from measurements made in the near-field, a transformation from one surface to another is necessitated. This transformation, of monochromatic but otherwise arbitrary waves can be accomplished efficiently by representing the field as a summation of any elementary wave solution of Maxwell's equations. Here, the coefficients to these solutions are determined by matching the fields on the surface on which the fields are known and by using mode orthogonality. Solving this modal expansion for the fields over a spherical surface of infinite radius centred about the radiator results in the far-field pattern. Generally, this is most effective when selecting a modal basis that is commensurate with the measurement geometry, *i.e.* by utilising plane-waves, cylindrical-waves, or spherical-waves respectively for the case where the measurements are taken over planar, cylindrical or spherical surfaces. Although complete solutions of the complex vector wave equation are available for certain other systems of co-ordinates, until relatively recently, these have received comparatively little attention in the published literature.

The utility and viability of any measurement system depends not only on the availability of the requisite probe-compensating near-field to far-field transformation, but also on the ease with which a sufficiently accurate robotic positioning sub-system can be constructed. The planar, cylindrical and spherical geometries have the inherent advantage that their respective robotic subsystems can be readily realised from combinations of readily available rotation, and/or linear translation stages at an economical price. Since it is possible to construct a right conical measurement system from any existing cylindrical system by merely tilting the linear stage (or alternatively by tilting the rotation axis), then this is also true for the conical case. Thus, the conical system can be conveniently fabricated using existing commercial off the shelf (COTS) positioning stages providing a solution for the characterisation of a class of antennas that currently can only be effectively served with spherical near-field scanning.

2. Overview of Measurement Technique & Transform

Conceptually, the right conical measurement system is perhaps most closely related to the well documented, well understood, cylindrical near-field scanning technique. Only here, the axis of rotation of the antenna under test (AUT) and the linear translation stage which caries the probe, are no longer constrained to be exactly parallel with one another. By taking samples incrementally on a raster grid by varying the azimuthal angle and linear displacement, the near electric-field can be sampled over the surface of a right cone. This is illustrated schematically in Figure 1 below.
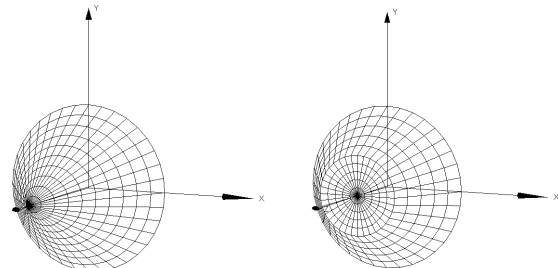

Figure 1 – Conical (left) & Frustum (right) Measurement Co-ordinate Systems.

If the near-field probe is rotated through 90° about its axis of rotation and this process is repeated, two orthogonal

near electric field components can be acquired and it is from these that the far-field pattern can be obtained. Previous transformation algorithms have been based on spherical, or plane wave expansions. In contrast, the near-field to far-field transform considered here is based upon a cylindrical mode expansion [5]. However, one assumption that has been introduced is that the probe is aligned such that it's axis of rotation is orthogonal to, and intersects with, the azimuthal (*i.e.* rotation) axis of the AUT. This has the benefit that the conventional cylindrical transmission matrix formula can be retained and when inverted, used to compensate the conical measurements without introducing any tangible practical limitations into the measurement process.

To provide an illustration of how this new transform works, let us consider obtaining the far-field pattern of a given radiator from cylindrical near electric field data sampled using an infinitesimal Hertzian dipole probe. This last restriction is introduced purely to simplify and ease the pedagogy and is not a fundamental constraint of the measurement technique. In summary, the electromagnetic fields outside an arbitrary test antenna radiating into free space can be expanded into a set of orthogonal cylindrical mode coefficients. These eigenfunctions can then be used to obtain the electric and magnetic fields everywhere in space outside of this conceptual cylindrical surface. Conveniently, these can be used to obtain explicit expressions for the asymptotic far-field pattern. When expressed in component from, the two sets of orthogonal cylindrical mode coefficients can be obtained from [5],

$$B_n^1(\gamma) = \frac{-1}{4\pi^2\kappa} \frac{1}{\acute{H}_n^{(1)}(\kappa\rho_0)} \int_{-\infty}^{\infty} \int_0^{2\pi} \left[\frac{n\gamma}{\rho_0} E_Z(\rho_0,\phi,z) \right. $$
$$ \left. + \kappa^2 E_\phi(\rho_0,\phi,z) \right] e^{-i(n\phi+\gamma z)} d\phi dz$$

And,

$$B_n^2(\gamma) = \frac{k_0}{4\pi^2\kappa} \frac{1}{H_n^{(1)}(\kappa\rho_0)} \int_{-\infty}^{\infty} \int_0^{2\pi} E_Z(\rho_0,\phi,z) e^{-i(n\phi+\gamma z)} d\phi dz$$

Where the Fourier variable can take on all real values from negative to positive infinity and the modal index can take on all integer values from negative to positive infinity. Here, ϕ and z denote the azimuthal and linear cylindrical co-ordinates respectively, ρ_0 is the radius of the measurement cylinder, k_0 is the free-space wave number, γ is the Fourier variable which is related to κ through $\gamma^2 = k_0^2 - \kappa^2$, and $H_n^{(1)}(z)$ is the Hankel function of the first kind. $\acute{H}_n^{(1)}(z)$ is the derivative of the Hankel function of the first kind which is defined using the following operator substitution [6],

$$\acute{H}_n^{(1)}(z) = \frac{d}{dz}\left(H_n^{(1)}(z)\right) = H_{n-1}^{(1)}(z) - \frac{n}{z}H_n^{(1)}(z)$$

Here, z has been used to denote the argument of the function. Finally, Hankel functions of the first kind of negative order can be calculated from Hankel functions of positive order from the following identity,

$$B_{-n}^1(z) = e^{i\pi|n|} B_{|n|}^1(z)$$

Once the cylindrical mode coefficients have been determined, the asymptotic far-field pattern can be obtained from a simple summation of modes as,

$$E_\theta\left(r \to \infty, \theta, \phi\right) = 2ik_0 \sin\theta \sum_{n=-\infty}^{\infty} (-i)^n B_n^2(\gamma) e^{in\phi}$$

$$E_\phi\left(r \to \infty, \theta, \phi\right) = -2k_0 \sin\theta \sum_{n=-\infty}^{\infty} (-i)^n B_n^1(\gamma) e^{in\phi}$$

Here, and as per the usual convention, the unimportant far-field spherical phase factor and inverse r term have been suppressed. In practice the number of cylindrical mode coefficients can be truncated to a finite number which equates approximately to half wavelength sampling over the surface of a conceptual cylinder that is centred on the origin of the measurement co-ordinate system, and that encloses the majority of the current sources. Thus, the maximum mode index N is given by $N = k_0 r_t + 10$ where r_t is the maximum radial extent (MRE) [7]. Also, the Fourier variable γ can be limited to $\pm k_0$ (equivalently, where $\kappa = 0$) as these are the highest order propagating modes. As the sample spacing, *i.e.* resolution, is determined from the maximum value of γ we can write that $\delta_z = \pi/k_0 = \lambda/2$ where λ denotes the wavelength.

Thus, for the conical case, the angular sample spacing is held fixed for all values of z at an amount determined by the size of the MRE, with samples being taken at every half wavelength along the linear scan axis, that is over the surface of the cone (*i.e.* not along the rotation axis where the two amounts differ be a factor of the cosine of the half cone angle).

From the analysis on the cylindrical case, it is clear that the cylindrical mode coefficients of the measured data depend upon the measurement radii in a fundamental way. Thus, unlike the conventional cylindrical case, it is not possible to represent the measured fields using just two sets of cylindrical mode coefficients; instead, two sets must be used for every value of ρ_0. In practice, this equates to computing a complete set of cylindrical mode coefficients for every ring of near-field data as this is the only case for which the value of ρ_0 will be held fixed. Thus, by computing the complete far-field pattern for each radial cut sequentially and then using the principle of linear superposition, the complete far-field pattern of the antenna can be constructed by essentially integrating over the set of near-field rings. Although not discussed herein, the probe pattern correction that is inevitably required when taking real near-field data can be incorporated into

this in a straightforward, but rigorous, way by using the usual inversion of the cylindrical transmission formula.

3. Preliminary Simulated Results

In order that the transformation algorithm outlined above could be verified, cylindrical and conical near-field measurement systems were simulated. The purpose of this was to allow the far-field patterns as obtained from the new transform algorithm to be compared with the far-field pattern as obtained directly from the modelled data. To this end, a proprietary three dimensional, full wave computational electromagnetic (CEM) solver employing the finite difference time-domain (FDTD) method was used to solve for the electric and magnetic fields in a problem space encapsulating a radiator. In this case, a simple open-ended rectangular waveguide (OEWG) section, excited by the fundamental TE_{10} mode was modelled. As the amount of computer memory required to solve problems such as this is closely related to the electrical size of the problem space, the Kirchhoff-Huygens principle, which is in essence a direct integration of Maxwell's equations, was used to calculate the radiated fields outside of the problem space, *c.f.* the Stratton-Chu solution [8]. Using this method, almost any form of near-field antenna measurement system irrespective of how large, could be simulated with a high degree of accuracy.

Figure 2 below contains the tangential E_ϕ and E_z amplitude field components over the surface of a cylinder shown in a three-dimensional "virtual reality" space. Figure 3 contains equivalent plots showing similar field components plotted over the surface of a truncated cone. In each of these simulations the main-beam of the antenna was aligned with the *z*-axis of the plot, *i.e.* through the side of the cylinder or frustum.
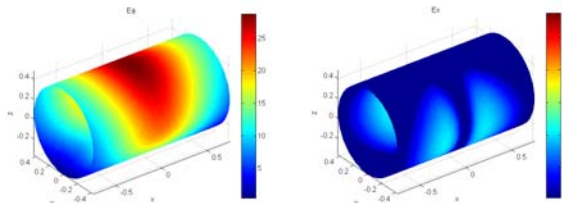

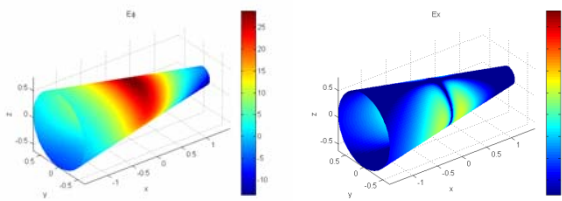**Figure 2 – Simulated Cylindrical Near-Field Data.**

Figure 3 – Simulated Conical Near-Field Data.

These simulated near-field measurements were then transformed to the true far-field using the algorithm described above and whereupon they could be compared with the predicted ideal patterns. The equivalent far-field

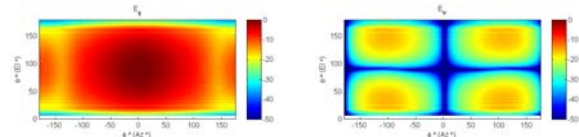patterns can be found presented in the form of false-colour, *i.e.* checkerboard, intensity plots.

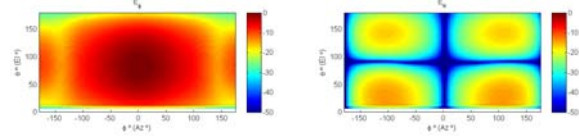

Figure 4 – Far-field Pattern From Cylindrical Data.

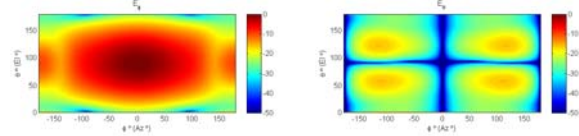
Figure 5 – Far-field Pattern From Conical Data.

Figure 6 – Far-field Pattern From Theoretical Model.

From inspection, the degree of agreement attained is encouraging with differences primarily resulting from the varying degrees of truncation within the simulated near-field data sets, which is evident in the broadening of the pattern in the elevation plane, the loss of field at large elevation angles, and the variation in the level of the "cross-polar" lobes – the far field pattern from the theoretical model being the only pattern free of truncation. As these preliminary results were viewed to be encouraging, particularly the agreement attained between the cylindrical and conical patterns, the work progressed to actual range measurements which are detailed in the sections below.

4. Preliminary Measured Results

The goal of this work was limited to demonstrating proof of concept where the success of this measurement technique was assessed by evaluating the repeatability between successive, preliminary, measurements where a single parametric change had been introduced. To this end, actual range measurements were taken using an NSI-200V-5x5 planar/cylindrical near-field measurement system with a precision tilting fixture that allowed for 0° or 30° half cone-angle, which is the angle between the local gravity vector and the linear axis. The AUT was an X-band standard gain horn (SGH) and multi-frequency data was taken from 8 to 12 GHz using an Agilent PNA-X based RF subsystem. The acquisitions were made using standard NSI 2000 cylindrical data acquisition software. This conical near-field system can be seen presented in Figure 7 below. Three different measurement cases were examined:

- Case 1 consisted of a conventional cylindrical near-field measurement and this was to be used as the

baseline measurement against which other test cases could be compared.

- Case 2 involved tilting the vertical axis of the scanner through 30° so that an equatorial conical near-field measurement was made. This case was selected so that the basic conical near-field to far-field transform could be verified against the baseline cylindrical case.

- Case 3 (illustrated in Figure 7) was intended to take advantage of the greater elevation coverage in order to improve the wide-out pattern coverage. In this configuration, the AUT was tilted up by 30° so that the boresight of the antenna was pointing towards the top of the conical measurement so that truncation would be lessened.

The goal of this measurement campaign was to obtain far-field patterns from cases 2 and 3 that agreed with those obtained from the baseline, *i.e.* Case 1.

Figure 7 – Conical Near-Field Measurement System.

The customised NSI-200V-5x5 planar / cylindrical measurement system, shown in Figure 7, was used to take near-field data for these three configurations. Plots of the measured amplitude of the principal polarisation can be seen presented as two-dimensional false-colour intensity plots in Figures 8, 9, and 10 below.

Since a cylindrical measurement can be considered to be a special case of the conical case, or *vice-versa*, the first, and possibly the simplest test, was to compare the conical transform against a reference cylindrical near-field to far-field transform to process the baseline Case 1 data set. Here, the well regarded National Institute of Standards and Technology (NIST) cylindrical near-field to far-field transform was used as the reference transform.
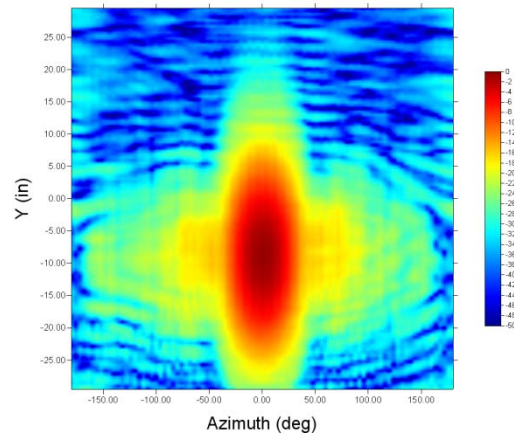
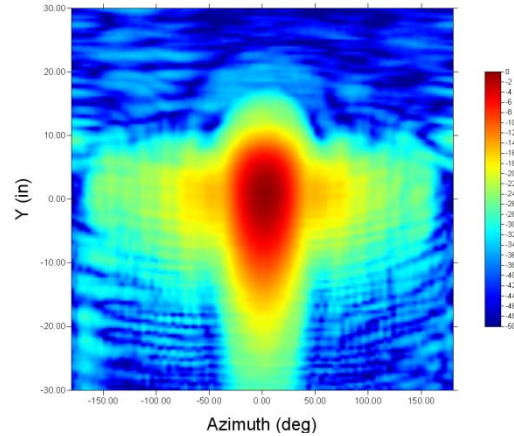

Figure 8 – Near-Field Amplitude Pattern of Case 1.

Figure 9 – Near-Field Amplitude Pattern of Case 2.
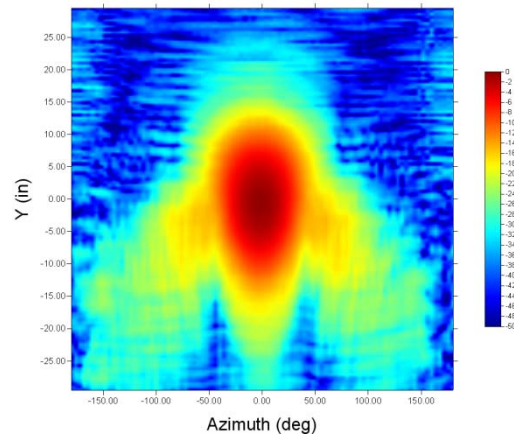

Figure 10 – Near-Field Amplitude Pattern of Case 3.

Figure 11 contains plots of the elevation cardinal cuts of the far-field antenna patterns which were obtained from the NIST transform with (red trace) and without (blue trace) probe pattern correction. Similar plots (which use the same colour convention) can be seen which were obtained from the novel conical near-field to far-field transform which can be seen to be in encouragingly good agreement with those patterns obtained from the NIST, *i.e.* reference, transform. Although not shown, the

agreement obtained between the respective azimuth cardinal cuts was equally good.
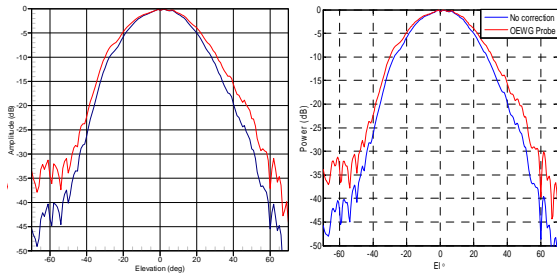

Figure 11 – Far-field Elevation Cuts, With & Without Probe Pattern Correction From The NIST Transform (Left) & The Novel Transform (Right).

As is evident from inspection of the plots of the near-field measured patterns, the data sets are all truncated to some degree in the nominally vertical linear axis which will inevitably lead to some leakage in the far-field pattern. Firstly, and as is the case with planar scanning, the first order truncation effect will result in the error within the pattern being effectively infinitely large outside of some angular limit which can be approximated by geometry (*c.f.* an infinite frequency, geometrical optics approximation). Secondly, the holistic nature of the relationship that exists between the near-field and far-field regions will result in the introduction of some ripple into the far-field pattern within even this angular range. Thus, when plotting these far-field patterns, fields outside of the first order truncation range have been omitted from the far-field false-colour plots, as evidenced by the white areas. Here, Figure 12 contains the far-field pattern from Case 1 – cylindrical measurement; Figure 13 contains the far-field pattern from Case 2 – conical measurement, whilst Figure 14 contains the far-field pattern obtained from Case 3 – conical measurement with tilted AUT. As Case 3 involves the measurement of an AUT which is not aligned with the axes of the range, *i.e.* the peak of the pattern is located at Az = 0°, El = 30°, a vector isometric rotation was utilised to rotate the antenna pattern so that it could be compared with the other, nominally aligned cases and the results of this can be found presented in Figure 15. This constitutes a full rotation of both the pattern and the polarisation so any differences that remain are not an artefact of any particular polarisation basis used to plot the patterns. A detailed description of this correction technique can be found in [9].

Here, it is evident that Figures 12, 13, and 15 are in encouraging agreement with one another giving further confidence that the near-field to far-field transform and probe pattern compensation are working correctly. It is worth noting that as the effects of the spatial filtering of the near-field probe depend upon the orientation of the probe and the AUT, Case 3 constitutes a stringent test for the transformation process as the patterns can only agree if the near-field to far-field transform, probe pattern

correction algorithm, probe pattern, and vector rotation are all implemented correctly. It is worth noting that due to the pattern rotation, the high elevation antenna pattern has *not* been filtered, and that the sharp lobe located at Az = 0°, El = 60° is the original pole in the far-field pattern, and as such this anomaly should be ignored. A similar comment is true for the lobe at Az =±180°, El =-60° which corresponds to the other pole.
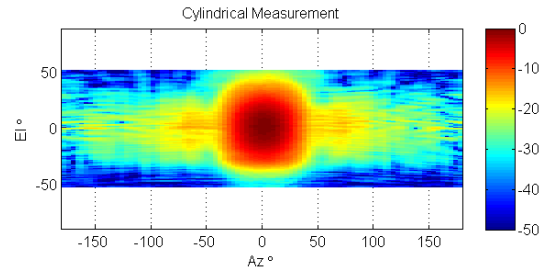

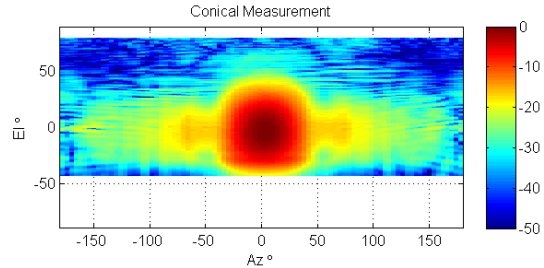**Figure 12 – Conventional Cylindrical Measurement.**

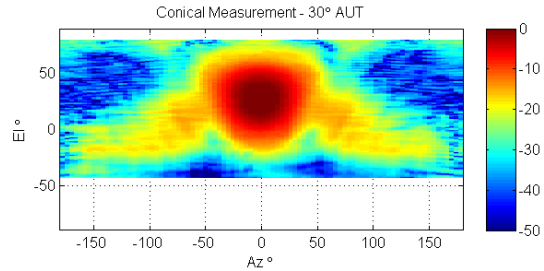**Figure 13 – Conventional Conical Measurement.**

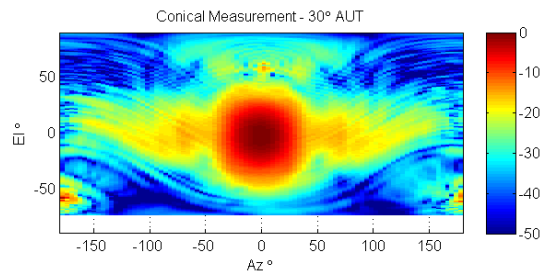**Figure 14 – Conical Measurement – tilted AUT.**

Figure 15 – Conical Measurement – Re-aligned AUT.

Since the success of this measurement technique is being assessed by evaluating the repeatability between successive measurements where a single parametric change has been introduced, the measurements must be very strictly controlled as any additional changes that are

introduced between successive measurements will affect the results. Unfortunately, as these measurements were preliminary in nature, they were not conducted within a screened anechoic environment and as such, the multi-path within the measurements did differ between each measurement configuration which degraded the agreement attained. This was particularly crucial as both the orientation of the AUT and the probe change between measurements. Crucially, the radii of the cylindrical, and particularly the conical, measurements was not accurately determined during these measurements which is the most likely cause of the small discrepancies in the location of the sidelobes in the alignment corrected Case 3 far-field patterns, *i.e.* Figure 15.

5. Discussion

Ideally, the boresight of the AUT would be orientated so that it points directly through the tip of the cone, *i.e.* in a polar mode (*c.f.* the equatorial mode measurements discussed herein) so that the undesirable effects of truncation are minimised. In practice however, any imperfection in the alignment of the conical system could result in the introduction of significant errors in the corresponding far-field pattern. This is a consequence of the fact that, naturally, the boresight direction of the AUT, and thus the region of greatest field intensity will be directed towards the tip of the cone, which is where the set of radial conical linear cuts intersect and where the alignment issues are most critical. Obviously, this can be eased by orientating the AUT so that it "looks" out through the side of the cone thus avoiding the tip region, but this is perhaps an inelegant solution. One alternative that has been used with considerable success in the closely related poly-planar measurement technique is to us a flat-topped measurement surface. For the poly-planar case a truncated pyramid, *i.e.* a pyramidal frustum, was employed to resolve this difficulty. Here however, an analogous conical frustum would be used which is a frustum created by slicing the top off a right cone where the cut is made parallel to the base of the cone. Here, the cap that is used to replace the tip of the conic section constitutes a conventional plane-polar measurement. It is intended to displace the intersection between the individual cuts from the region of greatest field intensity to a less sensitive location. Thus, in the event that the adjacent scans do not intersect perfectly, the resulting positional error will impact less on the far field pattern.

It is often preferable when taking near-field antenna measurements that a measurement geometry be selected which is commensurate with the geometry of the AUT. Thus, this technique would be particularly well suited to the characterisation of base-station antennas, or arrays installed behind tangent ogive radomes, such as those commonly employed with nose-mounted fire-control radars which is an electrically large system that often presents the experimentalist with both electromagnetic and mechanical challenges.

6. Conclusions and Future Work

This paper has recounted the use of a cylindrical mode expansion and an inversion of the cylindrical transmission formula as the basis of a novel probe-pattern corrected conical near-field to far-field transform for use with a conical near-field antenna measurement system where the validity of this novel approach has been demonstrated through numerical simulation and empirical measurement.

Finally, it should be noted that this paper recounts the progress of an ongoing research study. Consequently, several issues remain to be addressed and the planned future work is to include obtaining verification of the success of the right conic frustum measurement technique through further numerical simulation and actual range measurement.

7. REFERENCES

[1] S.F. Gregson, "Probe-Corrected Poly-Planar Near-Field Antenna Measurements", Doctoral Thesis, University of London, 2003.

[2] D. Leatherwood, "Conical Near-Field Antenna Measurement System", Antenna Measurements and Techniques Association (AMTA) symposium, St. Louis, November 2007.

[3] S.F. Gregson, C.G. Parini, J. McCormick, "Full Sphere Far-Field Antenna Patterns Obtained Using A Small Planar Scanner and a Poly-Planar Measurement Technique", AMTA, Austin Texas, October 2006.

[4] S.F. Gregson, C.G. Parini, J. McCormick, "Proposal For A Novel Near-Field Antenna Measurement Technique Employing A Conic Frustum Geometry", LAPC, Loughborough, March 2008.

[5] A.D. Yaghjian, "Near-Field Antenna Measurements On a Cylindrical Surface: A Source Scattering Matrix Formulation", NBS Technical Note 696, 1977.

[6] C.A. Balanis, "Advanced Engineering Electromagnetics", J. Wiley & Sons., 1989, pp. 936.

[7] J.E. Hansen (ed.), "Spherical Near-Field Antenna Measurements", The Institution of Engineering and Technology, UK, Peter Peregrinus Ltd., 1988.

[8] Silver S, "Microwave Antenna Theory and Design", First Edition 1947, McGraw Book Company Inc.

[9] S.F. Gregson, J. McCormick, C.G. Parini, "Principles of Planar Near-Field Antenna Measurements", The Institution of Engineering and Technology, UK, 2007.

ACKNOWLEDGEMENTS